Current Trends in Biotechnology and Pharmacy
Vol. 20 (Supplementry Issue 1A), March 2026, ISSN 0973-8916 (Print)., 2230-7303 (Online)
10.5530/ctbp.2026.1s.5


# Biosynthesis of Iron Oxide Nanoparticle Using *Adina Cordifolia*: *In Vitro* Evaluation of Antidiabetic Potential, Antioxidant, and Cytotoxic Effects

**Banuppriya Palani[1], Renu Vajjiravelu[1], Rajeshkumar Shanmugam[2], and Santhoshkumar Jayakodi[1]***

[1]Department of Biotechnology, Saveetha School of Engineering, Saveetha Institute of Medical and Technical Sciences, Chennai, Tamil Nadu 602105, India

[2]Nanobiomedicine Lab, Department of Anatomy, Saveetha Medical College and Hospital, Saveetha Institute of Medical and Technical Sciences, Chennai - 602105, Tamil Nadu, India

*Corresponding author: jksanthoshk@gmail.com

**Abstract**

Nanobiotechnology, a rapidly emerging field within nanomedicine, is gaining interest due to its potential to develop enhanced therapies. Further research is needed to improve the efficacy and safety of these medications. Synthesized *A. cordifolia* mediated Iron oxide nanoparticles (*A. cordifolia*-IONPs) were comprehensively characterized using various physicochemical techniques. UV-visible spectroscopy of the *A. cordifolia* plant extract exhibited distinct absorption red peaks at 400 and 430 nm. Then, synthesized IONPs with *A. cordifolia* exhibited distinct absorption peaks at 437 nm. Fourier-transform infrared (FTIR) spectroscopy, which showed distinctive bands at 3217 $cm^{-1}$, 2972.6 $cm^{-1}$, 1648.8 $cm^{-1}$, 1568 $cm^{-1}$, 1326 $cm^{-1}$, 1154.3 $cm^{-1}$, 1024.3 $cm^{-1}$, 825 $cm^{-1}$, 691 $cm^{-1}$, and 420 $cm^{-1}$ that were compatible with the synthesis of IONPs. X-ray diffraction (XRD) analysis showed that the material had an orthorhombic, average crystalline size of 36.06 nm, and a structural study showed that it had a smooth surface in spherical shape with a particle size of about 43.5 nm. A. cordifolia mediated IONPs inhibit α-amylase concentration-dependently, ranging from 30-77.4% (IC50 value of 26.360 µg/mL; 26.360 µg: R2 = 0.986). The β-glucosidase assay shows a dose-dependent inhibition range of 15.7-84.7% at concentrations of 10-50 µg/mL (IC50 25.705 µg/mL; $R^2$ 0.9433), with a statistically significant *** p-value < 0.0001. Followed by the antioxidant activity, and cytotoxic effect, as evaluated by the brine shrimp fatality experiment, was reduced. Exposed to greater amounts of the extract (40 and 80 µg/mL), the number of dead embryos was significantly ($p < 0.01$).

**Keywords:** *Adina cordifolia*, Iron (III) chloride, α-amylase, β-glucosidase, cytotoxic effect

## 1. Introduction

Nanotechnologies are an emerging discipline that has several uses in the food manufacturing, chemical, pharmaceutical, and cosmetic sectors (1). It is essential forl managing illnesses like cancer, heart disease, diabetes, and renal ailments, as well as for administering medicines, medical diagnostics (2). Nanoparticles are nanomaterials with a size between 1-100 nm. The nanoparticles of inorganic matter have gained interest because of their high surface area to volume ratio, specialized nature, and long-lasting release (3, 4). More than 50 years have passed since the first example of using nanotechnologies for drug delivery implementations, and we can today see how quickly focused drug delivery systems are developing (5, 6). The rapid development of sophisticated materials and nanotechnologies in recent years has created previously unthinkable opportunities in the fields of electronics, optics, materials science, and medicine (5, 7). One of the most significant uses of technology in medicine is undoubtedly the development of innovative therapeutic

Vol. 20 (Supplementry Issue 1A), March 2026, ISSN 0973-8916 (Print)., 2230-7303 (Online)
10.5530/ctbp.2026.1s.5

synthetic hybrids, nanotechnology-mediated diagnostic techniques, and nanosized component carriers for applications involving drug delivery (8, 9). The administration of drugs is the greatest prevalent aspect of nanomedicine, accounting for 76% of scholarly publications and 59% of patents (10). Metallic oxide nanoparticles have emerged as promising options in the therapeutic materials field recently due to their distinct chemical and physical properties and a wide range of applications (11).

The use of numerous green-synthesized plant-based nanoparticles is a new technique with unidentified potential medical uses. The modern age of nanomedicine has been ushered in by the improvement of medicinal uses of nanobiotechnology, which introduced the concept of employing nanomaterials to control and cure human biological systems (12). The efficacy of the administration of drugs depends heavily on the interactions of nanocarriers with living cells, making biocompatibility a critical factor. Research indicates that living things interact differently with nanostructured substances depending on their size, shape, surface charge, and functional categories (5). In order to reduce chronic side effects and the total quantity of medications, drug-packed nanoparticles can be precisely delivered to unhealthy tissue, such as malignant tumours, under the guidance of an external magnetic field. Injecting drugs into the vein of drug-loaded nanoparticles is now one of the most extensively studied methods for specialized drug administration (13). Drug delivery that is specific or magnetically regulated is made possible by nanoparticles of iron oxide (IONs). They have minimal toxicity, a high volume-to-surface ratio, and quick, affordable manufacture in addition to their superparamagnetic qualities. Drugs can be effectively encapsulated, adsorbed, conjugated, or dispersed by IONs (14). Super-paramagnetic iron oxide nanoparticles (SPIONs) have unique features, including minimal toxicity. As a result, they play a crucial role in various biological applications, including hyperthermia (15).

Type 2 diabetes mellitus (T2DM) is a severe pandemic health concern that affects over 420 million people worldwide. By 2040, it is expected to affect 642 million people. There are significant economic, social, and human costs associated with this rapidly spreading pandemic (16). Insulin resistance, variable degrees of overnutrition, inactivity, and resulting overweight or obesity cause islet β cells to fail to release enough insulin, resulting in type 2 diabetes, a chronic metabolic illness of fuel homeostasis. Fabricated oral hypoglycemia drugs and insulin are used to treat diabetes. However, they need daily administration, are costly, and have major adverse effects (17). Because of their nanometre size, they can pass through biological barriers and release medications gradually, enhancing diabetes management and lowering the need for frequent administrations (18). Additionally, IONPs have been studied for their ability to improve glucose homeostasis by altering important enzymes like α-amylase and β-glucosidase that are implicated in hyperglycemia after eating (19). Furthermore, found that SPIONs suppress most of the high-risk genes—PPAR-γ, IGF2BP2, WFS1, JAZF1, CAMK1D, PRC1, TCF7L2, and ZFAND6—that contribute to the possibility of type 2 diabetes in human primitive skeletal muscle (20). We have been creating a synthetic multifunctional platform for SPIONs over the past few years using polymers with good relaxing properties, relatively low toxicity, and blood biological compatibility. Maghemite (γFe2O3), a magnetic material with a rounded shape, makes up this particular design (21). The ROS, which includes the radical superoxide (O2•), hydroxyl radical (•OH), and hydrogen peroxide (H2O2), are continuously produced in the human body as a result of interactions with harmful chemicals in our surroundings and a variety of locally occurring metabolic pathways that make use of reactant enzymes (22).

Vol. 20 (Supplementry Issue 1A), March 2026, ISSN 0973-8916 (Print)., 2230-7303 (Online)
10.5530/ctbp.2026.1s.5

After that, in numerous biological reactions that are essential to life, such as the internal destruction of microorganisms by phagocytes, such as granulate cells and macrophages. Additionally, harmful radicals are being linked to several cellular signalling pathways known as redox signalling (23).

Although our body has built-in defences against oxidative stress, these become less effective as we age. This decrease increases the need for an ongoing intake of antioxidants that come from external sources, such as food or supplements. Proteins, lipoproteins, lipids, and DNA are among the essential macromolecules that reactive oxygen species (ROS) can easily harm. Anti-oxidant consumption, such as vitamin C, may reduce the possibility of malignancy, neurological illnesses, and heart problems, according to epidemiological research (24). Due to its capacity for carrying one electron, ferrous iron (Fe2+) can initiate a variety of radical reactions, even with comparatively non-active radicals (25). Since iron chelation has promise as a treatment strategy, the lack of highly efficient ligands is limiting its development. Finding a balance between the negative effects of chelators and their ability to defend against cellular oxidative stress is a crucial task. It has been shown that antioxidant-related therapies are effective in lowering oxidative damage. Red blood cells, in particular, benefit from these defense mechanisms (26).

The past few decades have seen a significant increase in interest in cancer early detection studies about the causal link between diabetes mellitus and cancer risk. There is growing indication that diabetes mellitus is linked to an increased risk of developing several cancers at several different locations, including endometrial, liver, and pancreatic carcinoma (27). A prior diagnosis of DM has been linked to an increased risk of OC in several cohorts and case-control studies; nevertheless, other pertinent investigations indicated a substantial negative connection. It is yet unknown when DM is linked to an elevated risk of OC due to confounding by obesity or high body mass index (BMI), as these conditions have been identified as risk factors for both DM and OC. Although new research has suggested a possible tight relationship between DM and OC, the epidemiological results between the two conditions are still up for dispute (28). Diabetic diagnoses have adverse effects on the ability to survive and are prognostic of OC patients. According to epidemiological research, persons with a history of diabetes are more likely to develop OC than the general population. The insulin-like growth factor class was discovered in diabetes patients and targeted a variety of pathways, including oxidative stress, angiogenesis, and tumor indicators (29).

Plant-based medications, which are made from biological sources, include a wide range of substances having pharmaceutical characteristics, and therapeutic plants are essential. The medicinal qualities of these bioactive components, which are frequently isolated from different plant parts like leaves, roots, bark, and flowers, have been used for the treatment and management of some illnesses (30).

*Haldinia cordifolia*, also known as *Adina cordifolia* (Roxb.) Hook.f. Ex Brandis (Rubiaceae) is an evergreen shrub that grows up to 900 meters in elevation in Indian tropical forests. It is used as an antiseptic, febrile agent, and bitter in ancient medicine. According to plant-based compounds analyses, saponins, phenolics, flavonoids, and tannins are present. In alloxan-induced diabetic rats, a hydro-alcoholic leaf extract showed notable antidiabetic action, confirming its ethnomedical application (31). The leaves of the *Adina cordifolia* (AC) plant are used traditionally as an antiseptic, febrifuge, and astringent. AC's bark-like roots had coumarins with antiamoebic properties, as did its thiosemicarbazone derivatives. Based on biochemical and spectral information, it was determined that AC included naringenin-7-methylether-40-O-α-L-rhamnopyranoside, a-amyrin, octacosanol, stigmasta-5, and 22-diene-3b-O-α-L4-b-rhamnopyranosyl-(1D xylopyranoside) (32). According to the previously reported *Prince*

Vol. 20 (Supplementry Issue 1A), March 2026, ISSN 0973-8916 (Print)., 2230-7303 (Online)
10.5530/ctbp.2026.1s.5

*Firdoos Iqbal et al*, the outer layer of bark is used to treat digestive problems and is bitter and caustic. Roots are employed to treat dysentery by acting as an irritant. The young stem of A. cordifolia has been tested for its anti-ulcer properties, and 7-hydroxycoumarin, which exhibited intriguing H+/K+ ATPase-inhibiting activities, was obtained by fractionating the chloroform extract using an enzymatic assay (33).

Traditional practitioners used *Adina cordifolia* to treat persistent coughing, jaundice, pain in the abdomen, fever, and Stomach inflammation. The roots are astringent and cause constipation, making them effective for both dysentery and diarrhoea. The bark is bitter, acrid, refrigerant, astringent, vulnerary, demulcent, diuretic, aphrodisiac, and tonic (34). It effectively treats pitta, wounds and ulcers, skin diseases, strangury, gastropathy, fever, and burning sensations. The buds are an antidote to snake venom, the blooms are used to treat headaches, and the leaves are used as an antiseptic in wound dressings (35). These are used to treat wounds, boils, and hemicrania. Adina cordifolia has a wide variety of therapeutic applications. It has antimicrobial, inflammatory, anti-aging, antinociceptive, and antifertility properties (34).

In the current objectives of the study, focus is on developing IONPs by green synthesis with aqueous extract of *A. cordifolia* root bark extract, and investigating the preliminary in vitro studies of evaluating the antidiabetic activity, zebrafish embryonic toxicology, and cytotoxic evaluation by using brine shrimp lethality assay of the IONPs.

## 2. Material methods

### 2.1. Materials

All of the materials, solvents, and reagents were purchased with high purity from Sigma Aldrich, Merck in Germany, for international companies, such as Iron (III) chloride ($FeCl_3$ ≥ *98.9%)*, 10X phosphate buffer, tris buffer, 6N hydrochloric acid, Alpha-amylase, Beta-glucosidase, Strach, Acarbose, and DNSA (3, 5 – 5-dinitrosalicylic acid ).

### 2.2 Collection of Plants

The *Adina cordifolia* Root bark was collected from the nearby Theni Forest in Tamil Nadu, identified, and authenticated by Dr. S. Mutheeshwaran, a scientist and botanist from St. Xavier's Research Foundation, St. Xavier's College, Palayamkottai-627 002. The Rubiaceae is the family to which *A. cordifolia* belongs. Following a double rinse with purified water, the gathered root bark was allowed to dry at room temperature. A voucher specimen (voucher no: XCH 40586) was deposited in the herbarium for future reference.

### 2.3. Preparation of the plant extract

Following thorough surface washing, the plants are finely ground using a mortar and pestle. One gram of powdered root bark was dissolved in 100mL of distilled water, heated for 20 minutes at 60° C on a heating mantle, allowed to cool to room temperature, and then filtered using No. 1 Whatman filter paper. The plant extract was stored in a refrigerator for the green synthesis of IONPs. The collected filtrates were then employed as stabilizing and reducing agents.

### 2.4. Preparation of the nanoparticles

The nanoparticle solution, which was prepared by mixing 30 mM of 0.486 g of iron chloride with 100 mL of distilled water, followed by the addition of 50 mL of plant extract and 50 mL of iron chloride solution, was incubated for 5 hours at 37°C and then for 24 hours at 450 rpm on a magnetic stirrer. The synthesized nanoparticles were visually confirmed and measured using a double-beam spectrophotometer when the fluid turned a dark block color. After the incubation, the sample was centrifuged for 10 minutes at 8000 rpm, and the collected pellet from the plant extract was mixed with the nanoparticle solution. The synthesized IONPs were dried overnight at 60°C in a hot air oven. For usage in biological applications and additional characterization, the *A. cordifolia*-IONPs pellet was collected and stored.

### 2.5. Characterization

Several techniques and tools were employed to characterize the *A. cordifolia*-

Vol. 20 (Supplementry Issue 1A), March 2026, ISSN 0973-8916 (Print)., 2230-7303 (Online)
10.5530/ctbp.2026.1s.5

mediated IONPs, verify their formation, and investigate their optical and physical properties. The color change of the synthesized mixture solution and the developed nanoparticles was visualized based on the reported value, which indicates the primary conformation of the Iron oxide nanoparticles. The absorbance of the *A. cordifolia*-IONPs was analyzed using a UV-visible spectrophotometer to scan across the range of 200-800 nm. To determine the functional group present in the developed NPs and drug-associated nanoparticles, as well as the biological substance involved in the *A. cordifolia* rootbark extract for nanoparticle formation, the FTIR spectrum of the bark extract, IONPs were evaluated in the spectrum of 4000 to 4oo $cm^{-1}$. An analysis using powder X-ray diffraction was conducted to ascertain the composition, Average crystalline size, and crystal structure of the IONPs. Dry powdered IONPs were adhered to glass slides using tape for SEM analysis. A JFC-1600 sputter coater was then used to apply a gold coating. The examination of the surface morphology and elemental composition of *A. cordifolia*-mediated IONPs was performed to a Quantax EDS attachment on a field-emission scanning electron microscope.

### 2.6. Antidiabetic Assay

#### 2.6.1. α-amylase antidiabetic assay

By determining maltose release, the α-amylase inhibitory activity was assessed. Green-synthesized *A. cordifolia*-mediated IONPs were pre-incubated with 100 µg/mL of α-amylase solution for 30 minutes at 37°C. The range of extract concentrations was 10 – 50 µg/mL; after that, an amount of starch (1% w/v; 100 µg/mL ) was added to the mixture, which was allowed to stand at 37°C for a further 30 minutes. Following that, 96-well plates, 3, 5 – 5-dinitrosalicylic acid (DNSA ) was added to stop the processes. A buffer made of sodium phosphate served as a control. By employing an ELISA plate detector, reflectance was determined at 540 nm.

#### 2.6.2. β-glucosidase Inhibitory assay

To investigate the β-glucosidase-inhibiting effect, a solution of starch (2% w/v) in 0.2 M tris buffer at pH 8.0 was mixed with 10–50 µg/mL of *A. cordifolia*-mediated IONPs. After adding 1 mL of β-glucosidase enzyme (1 U/mL), the resulting solution was incubated at room temperature for 40 minutes. The reaction was stopped with 2 mL of 6 N hydrochloric acid. Acarbose was used to serve a standard. The percentage of β-glucosidase inhibition was calculated by monitoring absorption at 540 nm using a plate reader for ELISA. The % of inhibition = C-T/C multiplied by 100, where T is the test sample and C is the control

### 2.7. Antioxidant Activity of *A. cordifolia*-mediated IONPs

#### 2.7.1. DPPH-radical scavenging activity

For ensuring the test's reliability and precision, a DPPH working solution (20 µM) was made from scratch in methanol using a 0.1 mM stock solution. Each well of a 96-well microplate received 200 µL of the DPPH working solution for the experiment. Next, in order to ensure uniformity, different concentrations of the A. cordifolia-mediated IONPs (10, 20, 30, 40, and 50 µg/mL) were added to the wells and gently mixed. To stop the DPPH radical from degrading too quickly, the combinations had to incubate for ten minutes at room temperature without light exposure. After incubation, the microplate reader was used to measure absorbance at 517 nm, using methanol as the blank. The following formula was used to determine the percentage of DPPH radical scavenging activity. Were, The formula for DPPH Scavenging Activity (%) is [(Absorbance control – Absorbance-sample) / Absorbance_control] × 100.

#### 2.7.2. H2O2- Free radical scavenging assay

The ability to scavenge H2O2 was evaluated for the biosynthesized A. cordifolia-mediated IONPs. We combined 40 mM H2O2 with a phosphate buffer that had a pH of 7.4. A solution of 0.6 mL H2O2 was mixed with the test sample (A. cordifolia-mediated IONPs) and a standard sample of ascorbic acid in different concentrations (10, 20, 30,

Vol. 20 (Supplementry Issue 1A), March 2026, ISSN 0973-8916 (Print)., 2230-7303 (Online)
10.5530/ctbp.2026.1s.5

40, and 50 µg/mL). Spectrophotometric measurement of the absorbance was performed at 230 nm following a 10-minute incubation period in a dark environment using vitamin C as using standard.

### 2.8. Zebrafish embryonic toxicology evaluation

#### 2.8.1. Fish maintenance and *A.cordifolia* mediated IONPs exposure

Five female and seven male adult zebrafish were employed to develop a breeding tank for the purpose of obtaining zebrafish embryos. After successfully mating, egg samples that were viable were collected and carefully cleaned, making sure to wash them at least three times using freshly made E3 media. fertilized eggs were then divided into six-well plates, each of which held two milliliters of fluid. Three sets of experimental and control groups were established for the study. Various amounts of freshly made stock solutions comprising *A. cordifolia*-mediated IONPs were added to the E3 media during the investigation. The sonic wave was applied to the solution for 15 minutes in order to maintain a pH range of 7.2-7.3 and produce homogeneous dispersion. It was given to healthily fertilizing eggs for 24 to 96 hours after fertilization at dosages ranging from 5 to 80 µg/mL. Every twelve hours, dead eggs were extracted from the groups that received A. cordifolia-mediated IONPs in order to avoid contamination. The testing plates were maintained at 28°C and covered with a layer of foil to lessen the effect of light interference.

#### 2.8.2. Zebrafish embryonic toxicology assessment

After being fertilized, the growth of zebrafish embryos was closely observed under a stereolens. Various quantities of A. cordifolia mediated IONPs, ranging from 5 to 80 µg/mL, including 5, 10, 20, 40, and 80 µg/mL, were administered to the embryos between 24 and 78 hours after fertilization. The study's primary objective was to evaluate the rates of embryonic death, egg hatching, and survival, all of which were monitored every 24 hours. An Ambala Cantt, India-based Coslab model HL-10A light microscope was used to document any anomalies found in the embryos and larvae in the control and treatment groups. Every 24 hours, a proportion of deformed embryos was recorded based on images of any malformed embryos (36).

### 2.9. Cytotoxic evaluation using the Brine shrimp lethality method

#### 2.9.1. Saltwater preparation

Two grams of iodine-free salt were added to 200 mL of distilled water and thoroughly mixed. 10- 12 mL of saline water was then patiently added to each well, and 10 nauplii were gradually added to each well. The previously prepared A. cordifolia mediated IONPs the added to each well at varying concentrations of 5, 10, 20, 40, and 80 µg/mL, and according to previous research, the sixth well served as a control, containing only salt water and living nauplii devoid of any sample. The ELISA plate was then incubated for about twenty-four hours.

### 2.10. Statistical analysis

The statistical analysis was carried out using GraphPad Prism (version 5.01). The two-way ANOVA test was employed to compare various groups. The mean ± SD is used to present the data, and p-values $< 0.05$ were statistically significant.

## 3. Result

### 3.1. Visual Observation

The aqueous iron (III) chloride solution first turned dark brown in color when the plant extract was added 1:1 concentration, indicating the development of an iron hydroxide intermediate for brown colour precipitate. The solution eventually turned black as the reaction progressed, indicating the reduction of Fe3+ ions and the subsequent formation of iron oxide nanoparticles. The formation of magnetite is characterized by this color shift from brown to black, in Figure 1, which is made possible by the extract's phytochemicals functioning as stabilizing and reducing agents.

Vol. 20 (Supplementry Issue 1A), March 2026, ISSN 0973-8916 (Print)., 2230-7303 (Online)
10.5530/ctbp.2026.1s.5

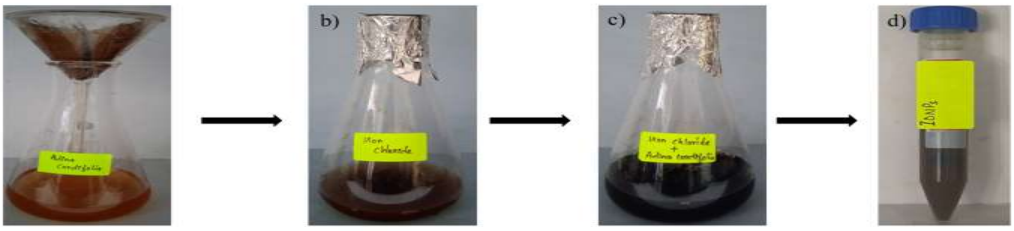


**Fig. 1:** Green synthesized IONPs using A. cordifolia root bark aqueous extract. a) Prepared plant extract after boiling the filtrate, b) precursor of Iron (III) chloride solution, c) 1:1 ratio of mixed plant extract and iron chloride solution, d) Finally, synthesized IONPs

$Fe_2Cl_3$ + $H_2O$ + Plant extract Fe (OH)3 (brown precipitate)
Fe (OH)3 Fe2 O3 (block color solution)

### 3.2. UV-Spectrum analysis

To further confirm the development of the IONPs, an ultraviolet-visible spectral analysis was utilized. Optical characteristics of green synthesized IONPs by using *A. cordifolia.* The IONPs were investigated using UV-Visible spectroscopy in the range of 200-800 nm. The absorption spectrum of the *A. cordifolia* plant extract displayed two predominant broad absorption red peaks at 400 and 430 nm. The plant extracts are characterized by π-π* electronic transitions due to the presence of polyphenolic compounds, flavonoids, and other phytochemical compounds. After that, biologically synthesized IONPs were successfully extracted with A. cordifolia, and a notable surface plasmon resonance band appeared with block peaks at 437 nm in Figure 2. This SPR peak verifies that ferric ions have been successfully reduced into a stable nanoparticle state and the distinctive optical property of IONPs nanoparticles. The phytochemicals interact with the nanoparticle surface during nucleation and development, which may result in a slight shift between the extract at 400 and 430 nm, ultimately explaining the 47 nm difference. During the development of metal and metal oxide nanoparticles, these phytoconstituents frequently act as organic stabilizing and reducing agents.

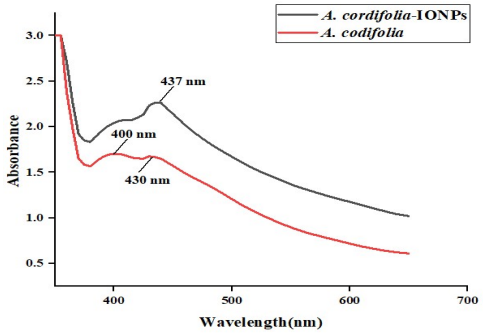


**Fig. 2**: UV – Visible spectral absorption of synthesized *A. cordifolia* mediated IONPs

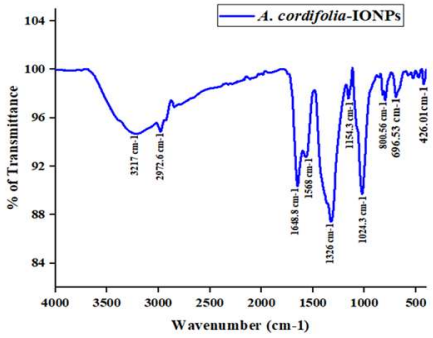


**Fig. 3**: Fourier transform infrared spectroscopy of aqueous extract of *A. cordifolia* root bark mediated IONPs

### 3.3. FTIR analysis of *A. cordifolia* mediated IONPs

The functional groups was used to examine FTIR spectroscopy found in the IONPs synthesized by using *A. cordifolia* root bark extract. Figure 3 Shows, FTIR spectrum

Vol. 20 (Supplementry Issue 1A), March 2026, ISSN 0973-8916 (Print)., 2230-7303 (Online)
10.5530/ctbp.2026.1s.5

| 3.4. Table 1 FTIR characterization of IONPs synthesized using *A. cordifolia* Root bark extract | | | |
|---|---|---|---|
| Wavenumber ($cm^{-1}$) | Functional group | Vibrational mode | Vibrational source |
| 3217 | O-H (amide) | Stretching | Free hydroxyl group, possibly amide O-H |
| 2972.6 | C-H | Asymmetric stretching | Aliphatic group of C-H (-CH3/-CH2) |
| 1648.8 | C-H | Bending | Aromatic compounds are commonly found in plants |
| 1568 | $-COO^-$ | Asymmetric stretching | Surface-bound carboxylate (COO-) |
| 1326 | O-H | Bending | Phenolic O-H bending |
| 1154.3 | C-O-C | Asymmetric stretching | Ether linkage (possibly flavonoid-derived) |
| 1024.3 | C-O | Symmetric stretching | Secondary alcohol or ester C-O |
| 800.56 | C-H | Bending | Aromatic compounds |
| 696.53 | Fe-O | stretching | Fe-O bond in iron oxide |
| 426.01 | Fe-O | Stretching | Metal-oxygen stretching in $Fe_2O_3$ |

of the noted absorption peaks were the synthesized IONPs. O-H stretching was represented by broad peaks observed at 3217 $cm^{-1}$, which suggested the presence of amide or free hydroxyl groups (30) . Aliphatic -CH3/ -CH2 groups, C-H asymmetric stretching vibrations were identified as the peaks at 2972.6 $cm^{-1}$. An absorption at 1648.8 $cm^{-1}$ corresponds to C-H bending, which is characteristic of plant-based aromatic compounds. Table 1 a peak at 1568 $cm^{-1}$, respectively -COO- stretching, was observed surface-bound to carboxylate groups. The phenolic group -O-H bending was observed by the peaks at 1326 $cm^{-1}$ (37). C-O-C asymmetric stretching was revealed by the absorption at 1154.3 $cm^{-1}$, which suggested the presence of the ether bonds. A peak at 1024.3 $cm^{-1}$ was associated with the secondary alcohol or esters stretching in a C-O symmetric form. The aromatic C-H bending bands are indicated by the absorption peaks at 800.56 $cm^{-1}$ (38). Finally, two significant peaks were observed at 696.56 and 426.01 $cm^{-1}$ in the spectrum, indicating and confirming the Fe-O vibrational stretching band, suggesting the formation of the IONPs (14). The aqueous extract of the *A. cordifolia* contains secondary metabolites that aided in the synthesis of the IONPs, as evidenced by this peak. The phenolic functional groups from the root bark extract provide the stability and capping of the nanoparticle at the surface.

### 3.5. X-ray diffraction analysis

The crystal phase of IONPs was evaluated using X-ray diffraction following the surface modification approach. The size of the nanoparticles for the plane-related data can be ascertained by applying the Debye-Scherrer equation, which is represented by equation 1, in addition to the information from the XRD pattern of the pertinent composition—identified crystal with the highest intensity of the diffraction.

$$D = 0.9 \lambda / \beta \cos \theta$$

In this relation, D is the crystal grain size in nanometres, λ is the X-ray wavelength, β is the width of the maximum peak at half its height, and θ is the angle at which the strongest peaks appear. The measurement of the wavelength of the crystallographic tool, which is given in degrees, needs to be translated to nanometers to determine the size of the nanocrystals. After choosing the peak in the XRD pattern with the highest intensity, 2θ, θ,

Vol. 20 (Supplementry Issue 1A), March 2026, ISSN 0973-8916 (Print)., 2230-7303 (Online)
10.5530/ctbp.2026.1s.5

and cosθ are computed for it. Furthermore, the formula β = (peak width × 3.14) / 180 yields the value of β in terms of radians. The size of the nanocrystals is determined in manometers by using the Debye-Scherrer equation (D = 0.9 λ / β cos θ) with the acquired data (39).

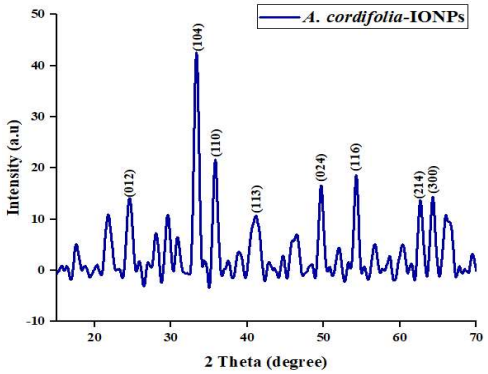


**Fig. 4**: XRD pattern for green-synthesized IONPs by using *A. cordifolia* root bark extract

Subsequently, Figure 4 displayed the XRD patterns of the synthesized *A. cordifolia*-mediated IONPs. The diffraction peaks were shown at 24.29, 33.28, 35.74, 40.97, 49.55, 54.23, 62.54, and 64.08 2θ, respectively, with (012), (104), (110), (113), (024), (116), (214), and (300) match the hk1 values (40). Synthesized *A. cordifolia* mediated IONPs crystal structure matches the standard card number (JCPDS card number 00-013-0534), suggesting that the bonding mechanism of IONPs remained unchanged. The average crystalline size of *A. cordifolia*-mediated IONPs was determined using the standard Debye-Scherer equation. The *A. cordifoila*-mediated IONPs have an average crystal size of 43.5 nm, and then rhombohedral crystal system, respectively.

### 3.6. SEM with EDX analysis

The morphological features of the nanoparticle were shown in detail by SEM images. Figures 5 A) and B show the smooth surface morphology, which shows that the

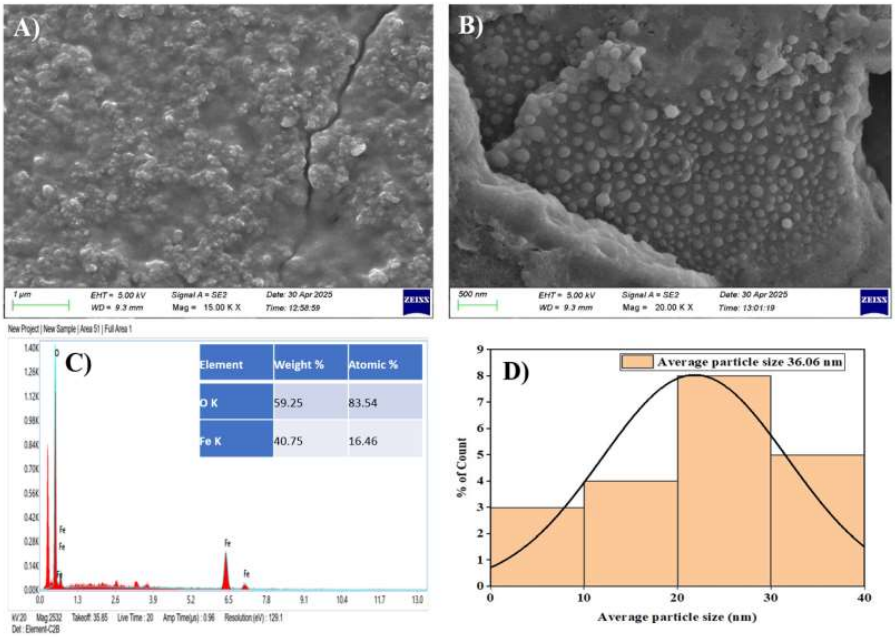


**Fig. 5**: For synthesized *A. cordifolia* mediated IONPs, A) SEM images with 15 k magnification of IONPs, B) SEM images with 20 k magnification of IONPs, C) EDX analysis of IONPs, D) Average particle size 36.06 nm

Vol. 20 (Supplementry Issue 1A), March 2026, ISSN 0973-8916 (Print)., 2230-7303 (Online)
10.5530/ctbp.2026.1s.5

nanoparticles are spherical and aggregated (41). The size of the nanoparticle is approximately 36.06 nm and exhibits a variable distribution, as shown in Figure 5D. The investigation verified the presence of IONPs, indicating that IONPs prepared using *A. cordifolia* extract contain the constituents Fe and O, along with trace amounts of minerals. Figure 5 C) shows the weight percentages of the EDS table shown in the insert, 40.75% for iron and 59.25% for oxygen, and then trace amounts are present in potassium.

### 3.7. Antidiabetic assay

As illustrated in Figure 6 *A cordifolia*-mediated IONPs showed significant inhibitory effects on β-glucosidase and α-amylase enzyme activity in anti-diabetic evaluations. The dose-dependent decline in enzyme activity suggests a potential mechanism for glycemic control. Tannic acid-alginate's inhibition of α-amylase points to a reduction in the breakdown of complex carbohydrates, which in turn leads to a decrease in the production of glucose. The simultaneous observation of β-glucosidase inhibition suggests a potential change in the way glucose is absorbed in the small intestine. The potential of tannic acid-alginate to alter glucose absorption and carbohydrate degradation is revealed by using acarbose as a benchmark for comparative study. The overall findings suggest the potential use of synthetic tannic acid-alginate for further studies in the area of antidiabetic treatments, indicating that the compound may help lower postprandial hyperglycemia.

#### 3.7.1. α-amylase Inhibitory assay

In Figure 6, at various concentrations of 10, 20, 30, 40, and 50 µg/mL, *A. cordifolia* mediated IONPs showed a dosage-dependent inhibitory effect, as shown in Figure 6. On the other hand, the conventional acarbose showed % between 30-83.7% at the right levels (IC50 value of 26.360 µg/mL; 26.360 µg: R2 = 0.986). The α-amylase enzyme inhibitory activity can be used for type 2 diabetes mellitus.

#### 3.7.2. β-glucosidase Inhibitory assay

As shown in Figure 7 *A, Cordifolia*-mediated IONPs likewise showed concentration-dependent inhibition at dosages of 10, 20, 30, 40, and 50 µg/mL, with percentages of 15.7%, 45.2%, 63.2%, 77.6%, and 84.8%, respectively. These results demonstrate can alter α-amylase activity and that the herbal extract affects their inhibitory qualities. The β-Glucosidase inhibitory test for

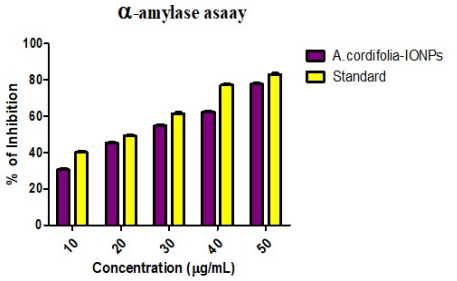


**Fig. 6**: Graphical presentation of the antidiabetic activity of *A. cordifolia*-IONPs α-amylase assay, the images represent data expressed using Two-way ANOVA with GraphPad Prism version 5.0, statistically analyzed p-value < 0.0001, it is statistically significant ** *: p < 0.0001.

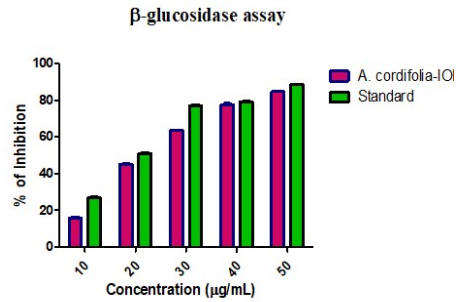


**Fig. 7**: Graphical presentation of the antidiabetic activity of *A. cordifolia*-IONPs β-glucosidase assay, the images represent data expressed using Two-way ANOVA with GraphPad Prism version 5.0, statistically analyzed p-value < 0.0001, it is statistically significant ** *: p < 0.0001.

Vol. 20 (Supplementry Issue 1A), March 2026, ISSN 0973-8916 (Print)., 2230-7303 (Online)
10.5530/ctbp.2026.1s.5

this enzyme was examined in this work. The $IC_{50}$ result for the *A. cordifolia* mediated IONPs was 25.705 µg/mL ($IC_{50}$ 25.705 µg/mL; $R^2$ 0.9433). These findings support the *A. cordifolia* mediated IONPs possible antidiabetic qualities and help to explain the β-glucosidase inhibitory effects they have been shown to exhibit. Effective antidiabetic potential was demonstrated by the *A. cordifolia*-mediated iron oxide nanoparticles (IONPs), which showed greater α-amylase inhibitory effects than β-glucosidase. The dose-dependent raised α-amylase and β-glucosidase inhibitory activity was similar to that of the common medication, acarbose.

### 3.8. Free Radical Scavenging activity

#### 3.8.1. DPPH-scavenging inhibitory assay

In Figure 8, at different dose concentrations of *A. cordifolia* mediated IONPs at 10, 20, 30, 40, and 50 µg/mL showed a dose-dependent inhibitory effect. The antioxidant activity of IONPs, assessed by using the DPPH radical scavenging assay, demonstrated the highest inhibition at 50 µg/mL, 70.6 % and the lowest inhibition at 10 µg/mL, 29.1 % (IC50 value of 31.3 µg/mL; 31.3 µg: R2 = 0.9823) of the DPPH assay. Two-way measures ANOVA revealed highly significant effects of time, *p-value* < 0.0001, column factor (*p* = 0.0017), and subject variability was also significant (*p* = < 0.0001).

#### 3.8.2. H2O2-scavenging activity

The antioxidant efficacy of *A. cordifolia*-mediated IONPs was evaluated using the H2O2 assay in Figure 9. Using vitamin C ascorbic acid as the basis for comparison, the H2O2 assay of IONPs shows the maximum concentration of inhibition at 50 µg/mL, of 71.6%. At the lowest concentration of IONPs at 10 µg/mL, the 30.2 % H2O2 assay. The statistics were measured at Two-way ANOVA revealed highly significant effects of time, *p-value* <0.0001 column factor (*p* = 0.0003), and subject variability was also significant (*p* = 0.0001).

### 3.9. Zebrafish Embryonic Toxicology Evaluation

The Zebrafish embryonic survival was 60% when exposed to 80 µg/mL of an *A. cordifolia*-mediated IONPs, and it increased to 80% when exposed to 20 and 40 µg/mL. However, 100% vitality was observed in the groups receiving treatment at 5 and 10 µg/mL, as well as in the blank control group Figure 10. There were no noticeable changes ($p > 0.05$) when administering dosages of 20 and 40 µg/mL. However, embryo mortality was dramatically impacted ($p < 0.01$) when the bio-composite concentration was increased to 40 and 80 µg/mL. The morphological observation revealed zebrafish embryos that were partially formed on the first day, according to morphology assessments. Day 2 saw the complete development of the embryos, and day three saw the successful hatching of perfectly developed young zebrafish. There are no structural abnormalities, such as bending of the spine or tail, or indications of oedema in Figure 11.

The percentage of embryos that were

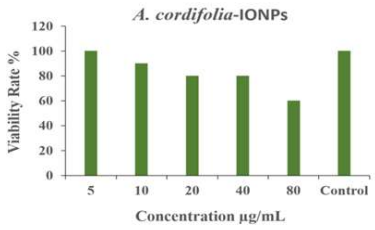


**Fig. 8**: Graphical presentation of antioxidant activity of *A. cordifolia*-IONPs in DPPH assay

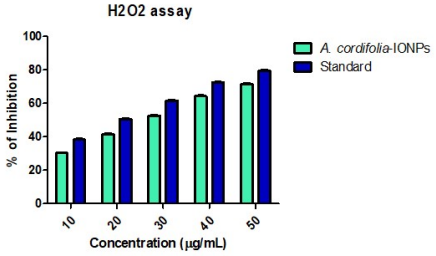


**Fig. 9**: Graphical presentation of antioxidant activity of *A. cordifolia*-IONPs in H2O2 assay

Vol. 20 (Supplementry Issue 1A), March 2026, ISSN 0973-8916 (Print)., 2230-7303 (Online)
10.5530/ctbp.2026.1s.5

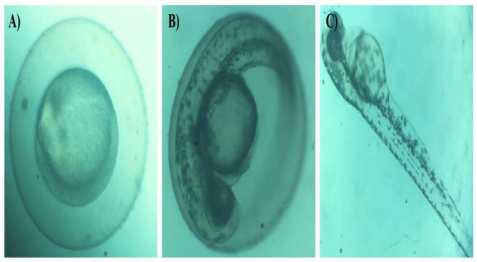


**Fig. 10**: Schematic presentation of a microscopic image of wild zebrafish embryonic toxicology imaging of *A. cordifolia*-IONPs. A) First day images show partial signs of healthy developed embryos inside the egg, B) Second day images showed well-developed, healthy zebrafish inside the egg, C) Third day showed 80% hatched, healthy zebrafish

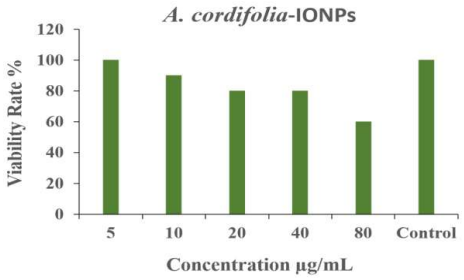


**Fig. 11**: Graphical presentation of 76-hour zebrafish embryo viability rates following exposure to varying doses of *A. cordifolia*-IONPs

successfully hatched at *an A. cordifolia*-mediated IONPs concentration of 80 and 40 µg/mL was 80%. A 20 µg/mL concentration was 90% of the hatching rate of *A. cordifolia* mediated IONPs. The hatching rate was 100% at both 5 and 10 µg/mL concentrations of *A. cordifolia*-mediated IONPs; in contrast, the blank control had a 100% hatching rate. The concentrations also affected the rate of zebrafish embryo hatching, as seen in Figure 12. The untreated embryos hatched 100% of the time. However, embryos showed an 80% hatching rate at extract concentrations of 80 and 40 µg/mL. No

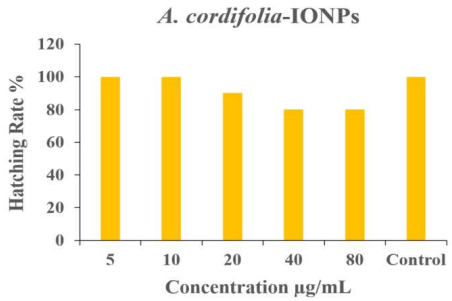


**Fig. 12**: Graphical presentation of the hatching rates of zebrafish embryos 76 hours after exposure to varying concentrations of *A. cordifolia*-IONPs

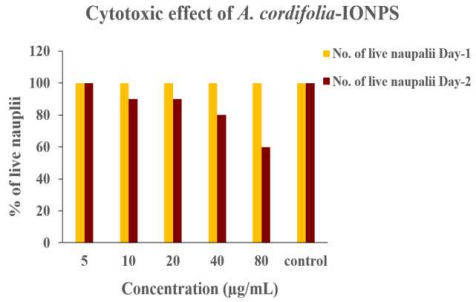


**Fig. 13**: Graphical presentation of the cytotoxic evaluation of *A. cordifolia* mediated IONPs using the brine shrimp lethality assay

discernible difference existed between the two concentrations. The p-value for them was less than 0.01. Nonetheless, the hatching percentage was deemed reasonably significant if < 0.05 was present.

### 3.10. Cytotoxic Evaluation

The brine shrimp lethality experiment was used to evaluate the cytotoxic effects of the *A. cordifolia*-mediated IONPs, as shown in Figure 13. This method is often used to measure a substance's impact on the survival of brine shrimp nauplii, assessing its cytotoxicity. To show the percentage of live nauplii, a drug-free control group was maintained for the current investigation. The findings of the cytotoxicity evaluation demonstrated that the *A. cordifolia*-mediated

Vol. 20 (Supplementry Issue 1A), March 2026, ISSN 0973-8916 (Print)., 2230-7303 (Online)
10.5530/ctbp.2026.1s.5

IONPs had varying effects on the presence of nauplii at varying doses. The assessment of the cytotoxic effect indicated that different concentrations of *A. cordifolia*-mediated IONPs exhibited varying impacts on live nauplii. 60 live nauplii were collected and equally distributed with 10 nauplii per well. The effect of IONPs was evaluated at 24-hour duration. All sixty nauplii lived on the first day for all concentrations 5-80µg/mL. Similarly, 100% of the nauplii survived when exposed to control as well as 5 µg/mL of the *A. cordifolia* with IONPs on day 2. However, 90% of the nauplii lived at doses of 10 and 20 µg/mL. 80% of the nauplii survived at a 40 µg/mL concentration. In addition, 60% of the nauplii survived when the concentration was raised to 80 µg/mL. The effect of the *A. cordifolia-mediated* IONPs was evaluated at 48h intervals.

## 4. Discussion

The current investigation sought to evaluate and examine the possible antidiabetic effects and embryonic toxicology, and cytotoxic effects of IONPs produced in an environmentally friendly manner through the use of herbal formulations containing A. cordifolia root bark extract. The study included the synthesis procedure, visual inspection, UV-visible spectrophotometry characterisation, and ensuing in vitro antidiabetic tests that targeted the enzymes α-amylase and β-glucosidase. Employing extracts from *A. cordifolia* as a naturally occurring reduction and stabilising agent, green-synthesized iron oxide nanoparticles (IONPs) were effectively created. Their characteristics were assessed using a variety of characterisation methods as well as visual examination. The *A. cordifolia*-IONPs solution started out dark brown (Figure 1) and eventually turned dark, signifying that the synthesis process was complete. This noticeable colour change verified that the environmentally friendly *A. cordifolia* extract had reduced iron ions. The plant extract of A. cordifolia exhibited two prominent, broad absorption red peaks at 400 and 430 nm in its absorption spectrum. Because of the presence of flavonoids, polyphenolic chemicals, and other phytochemical substances, the plant extracts exhibit π-π* electronic transitions. Following the effective extraction of biologically synthesised IONPs using A. cordifolia, a prominent surface plasmon resonance band with block peaks at 437 nm was observed. Although considerable aggregation was observed, scanning electron microscopy (SEM) revealed a spherical morphology with an average particle size of approximately 36.06 nm. The successful synthesis of IONPs using *A. cordifolia* extract was validated by energy-dispersive X-ray (EDX) analysis, which further corroborated the elemental composition, revealing potassium, oxygen, and iron as the major elements. The present study assessed the antidiabetic and cytotoxic effects of an A. cordifolia-mediated IONPs.

Previously reported, we assessed SPIONs' potential anti-diabetic effects in rats with streptozotocin-induced diabetes and contrasted them with the effects of metformin therapy (15). Another investigation shows that QCSPIONs were more effective than pure QC in improving learning and memory in diabetic rats. This is the first study that we are aware of that examines QCSPIONs in relation to cognitive impairment caused by diabetes. Multiple low-dose STZ injections were used to develop type 1 diabetes, which led to decreased body weight and raised blood glucose levels. The effective generation of the diabetic model was validated by histological investigation after 45 days, which revealed widespread destruction to Langerhans islets and pancreatic beta cells (42).

A prior work used *Madhuca indica* extract to create iron oxide nanoparticles (FeONPs) in a green way. SEM revealed that the particles had an average size of 56 nm, and biological experiments showed significant antidiabetic (73.26% α-amylase), anti-inflammatory (96.20% inhibition), and antioxidant (81% DPPH) properties. The results of the in silico ADMET research showed promising therapeutic qualities. Additional safety evaluations are necessary to confirm their abilities for use in biological

Vol. 20 (Supplementry Issue 1A), March 2026, ISSN 0973-8916 (Print)., 2230-7303 (Online)
10.5530/ctbp.2026.1s.5

scenarios (43). The investigation, the antioxidant activity of developed IONPs by using *A. cordifolia,* revealed that the DPPH was assessed at the highest concentration at 50 µg/mL, 70.6 % and the lowest inhibition at 10 µg/mL, 29.1 % IC50 value of 31.3 µg/mL. Another study examined the possible antidiabetic effects of green-synthesised iron oxide ($Fe_2O_3$) nanoparticles made with stem extract from *Securidaca longipedunculata*. The nanoparticles were tested in alloxan-induced diabetic albino Wistar rats. After receiving $FeO_3$ nanoparticle treatment for 21 days, blood glucose levels dropped dramatically ($p<0.05$) from 409.50±5.50 to 199.15±9.33 mg/dL, and body weight improved considerably (44).

This previous study used a gestational diabetes mellitus (GDM) model to investigate the diabetes-preventing and liver-protective effects of Panicum repens-mediated iron nanoparticles (FeNPs). The green-synthesised FeNPs had a spherical shape and showed promise in enhancing liver function and lowering blood glucose levels. FeNP treatment also helped to alleviate changes brought on by diabetes and restore hepatic structure. According to these results, FeNPs show promise as an adjuvant treatment for GDM management that also protects the liver (45).

The earlier study showed that α-amylase inhibiting assays used in CuONPs had concentration-dependent action, with inhibition varying between 40% and 77% at doses between 10 and 50 µL. Likewise, the β-glucosidase test revealed inhibition ranging from 53% to 79%, suggesting powerful diabetes prevention efficacy via enzymatic regulation. The range of α-amylase and β-glucosidase inhibitions for ZnONPs made with *lemongrass* and *mint* formulations was 36% to 80% and 50% to 78%, respectively. These results indicate the potential of both nanoparticles in antidiabetic treatment by demonstrating their strong inhibitory effects on important enzymes involved in the metabolism of carbohydrates (46).

The current investigation showed that *A. cordifolia* mediated had a moderate level of antioxidant activity. The developed IONPs demonstrated improved antioxidant potential at lower concentration and attained activity comparable to the standard at higher concentration, according to the H2O2 assay.

The findings of the brine shrimp lethality assay (BSLA) showed that an ethanolic extract *of C. bonplandianum* had a cytotoxic impact that was dependent on extract concentration. While higher concentrations caused a steady loss in viability, lower amounts had little effect on nauplii survival. These results demonstrate the extract's efficacy against brine prawns by pointing to the existence of biologically active substances with cytotoxic ability (47).

Previous studies have concentrated on employing the plant *Mimosa pudica* to synthesise strontium nanoparticles in an environmentally friendly and sustainable manner. The cytotoxic properties of these nanoparticles on cancerous cells and their anti diabetic action have demonstrated encouraging outcomes. The alpha-amylase inhibitor assay was used in this work to examine the antidiabetic impact, while the brine shrimp lethality assay was used to examine the cytotoxic effect. Similarly to the standard employed, acarbose, increasing concentrations of *Mimosa pudica*-mediated strontium nanoparticles showed increased cytotoxic and antidiabetic effects during these experiments (48).

## 5. Conclusion

The results of the investigation showed that iron oxide nanoparticles (IONPs) made with extract from *A.cordifolia* have strong antidiabetic potential. The concentration-dependent inhibition of α-amylase and β-glucosidase, two important enzymes that break down carbohydrates, emphasizes their therapeutic significance in the treatment of diabetes. Their initial biocompatibility for biomedical applications was further supported by cytotoxic evaluation utilizing the brine shrimp lethality assay,

Vol. 20 (Supplementry Issue 1A), March 2026, ISSN 0973-8916 (Print)., 2230-7303 (Online)
10.5530/ctbp.2026.1s.5

which showed comparatively minimal toxic effects at tested dosages. Future research is necessary to examine the potential of *A. cordifolia*-mediated IONPs in the prevention and treatment of diabetes related ovarian cancer. Clarifying molecular pathways, performing in vitro and in vivo evaluations, and assessing their effective component are incorporated into nanomedicine-based therapeutics, should be the main goal of such investigations.

**Declaration of Competing Interest**

The authors declare no financial or personal interests that could have influenced the work presented in this study

**References**

1) Malik S, Muhammad K, Waheed Y. (2023). Nanotechnology: a revolution in modern industry. Molecules; 28(2):661.
2) Malik S, Muhammad K, Waheed Y. (2023). Emerging applications of nanotechnology in healthcare and medicine. Molecules; 28(18):6624.
3) Susaimanickam A, Selvaraj D, Manickam P. (2024). Nanoparticle-based bioremediation of organic and inorganic substances from water bodies. Bioremediation of Emerging Contaminants in Water Volume 2: ACS Publications; . p. 135-62.
4) Jayakodi S, Senthilnathan R, Swaminathan A, Shanmugam VK, Shanmugam R, Krishnan A, et al. (2023). Bio-inspired nanoparticles mediated from plant extract biomolecules and their therapeutic application in cardiovascular diseases: A review. International Journal of Biological Macromolecules; 242:125025.
5) Nasrollahi S, Alizadeh N. (2024). Synthesis of functionalized superparamagnetic iron oxide nanoparticles for ibuprofen and naproxen hydrophobic drugs delivery. Materials Chemistry and Physics; 326:129775.
6) Jayakodi S, Kim H, Menon S, Shanmugam VK, Choi I, Sekhar MR, et al. (2022). Preparation of novel nanoformulation to enhance efficacy in the treatment of cardiovascular disease. Biomimetics; 7(4):189.
7) Rokunuzzaman MK. (2024). The Nanotech Revolution: Advancements in Materials and Medical Science. Journal of Advancements in Material Engineering; 9(2):1-10.
8) Nasir A, Khan A, Li J, Naeem M, Khalil AA, Khan K, et al. (2021). Nanotechnology, a tool for diagnostics and treatment of cancer. Current topics in medicinal chemistry; 21(15):1360-76.
9) Jayakodi S, Shanmugam VK. (2021). Statistical optimization of copper oxide nanoparticles using response surface methodology and Box–Behnken design towards in vitro and in vivo toxicity assessment. Biointerface Research in Applied Chemistry; 11(3):10027-39.
10) Turrina C, Klassen A, Milani D, Rojas-González DM, Ledinski G, Auer D, et al. (2023). Superparamagnetic iron oxide nanoparticles for their application in the human body: Influence of the surface. Heliyon; 9(6).
11) Nikolova MP, Chavali MS. (2020). Metal oxide nanoparticles as biomedical materials. Biomimetics; 5(2):27.
12) Shanmugam R, Govindharaj S, Arunkumar P, Sanjana GS, Manigandan P. (2024). Preparation of a herbal mouthwash with lemongrass and mint-mediated zinc oxide nanoparticles and evaluation of its antimicrobial and cytotoxic properties. Cureus; 16(2).
13) Shanmugam R, Deenadayalan P, Manigandan P. (2024). Anticariogenic, antidiabetic, and toxicology evaluation of the ethanolic extract of Croton bonplandianum: An in vitro study. Cureus; 16(7).
14) Atabaki H. (2024). Synthesis of iron oxide magnetic nanoparticles and chitosan biopolymer in aqueous solutions. Inorganic Chemistry Communications; 162:112161.
15) Ali LM, Shaker SA, Pinol R, Millan A, Hanafy MY, Helmy MH, et al. (2020). Effect of superparamagnetic iron oxide nanoparticles on glucose homeostasis on type 2 diabetes experimental model. Life sciences; 245:117361.
16) Norouzi M, Norouzi S, Ruggiero A, Khan MS, Myers S, Kavanagh K, et al. (2021). Type-2 diabetes as a risk factor for severe

COVID-19 infection. Microorganisms; 9(6):1211.
17) Aljulifi MZ. (2021). Prevalence and reasons of increased type 2 diabetes in Gulf Cooperation Council Countries. Saudi Medical Journal; 42(5):481.
18 Souto EB, Souto SB, Campos JR, Severino P, Pashirova TN, Zakharova LY, et al. (2019). Nanoparticle delivery systems in the treatment of diabetes complications. Molecules; 24(23):4209.
19) Seo D-H, Yoo S-H, Choi S-J, Kim Y-R, Park C-S. (2020Versatile biotechnological applications of amylosucrase, a novel glucosyltransferase. Food science and biotechnology; 29(1):1-16.
20) del Bosque-Plata L, Martínez-Martínez E, Espinoza-Camacho MÁ, Gragnoli C. (2021). The role of TCF7L2 in type 2 diabetes. Diabetes; 70(6):1220-8.
21) Alsenousy AH, El-Tahan RA, Ghazal NA, Piñol R, Millán A, Ali LM, et al. (2022). The anti-obesity potential of superparamagnetic iron oxide nanoparticles against high-fat diet-induced obesity in rats: possible involvement of mitochondrial biogenesis in the adipose tissues. Pharmaceutics; 14(10):2134.
22) Engwa GA, Nweke FN, Nkeh-Chungag BN. (2022). Free radicals, oxidative stress-related diseases and antioxidant supplementation. Alternative Therapies in Health & Medicine; 28(1).
23) Sadiq IZ. Free radicals and oxidative stress: (2023). Signaling mechanisms, redox basis for human diseases, and cell cycle regulation. Current molecular medicine; 23(1):13-35.
24) Doseděl M, Jirkovský E, Macáková K, Krčmová LK, Javorská L, Pourová J, et al. (2021). Vitamin C—sources, physiological role, kinetics, deficiency, use, toxicity, and determination. Nutrients; 13(2):615.
25) Thor S-H, Ho L-N, Ong S-A, Abidin CZA, Heah C-Y, Yap K-L. (2023). Disclosing the mutual influence of photocatalytic fuel cell and photoelectro-Fenton process in the fabrication of a sustainable hybrid system for efficient Amaranth dye removal and simultaneous electricity production. Environmental Science and Pollution Research; 30(12):34363-77.
26) Majeed S, Danish M, Mohamad Ibrahim MN, Sekeri SH, Ansari MT, Nanda A, et al. (2021). Bacteria mediated synthesis of iron oxide nanoparticles and their antibacterial, antioxidant, cytocompatibility properties. Journal of Cluster Science; 32(4):1083-94.
27) Huang J, Chan WC, Ngai CH, Lok V, Zhang L, Lucero-Prisno III DE, et al. (2022). Worldwide burden, risk factors, and temporal trends of ovarian cancer: a global study. Cancers; 14(9):2230.
28) Wang L, Zhong L, Xu B, Chen M, Huang H. (2020). Diabetes mellitus and the risk of ovarian cancer: a systematic review and meta-analysis of cohort and case–control studies. BMJ open; 10(12):e040137.
29 Karimi F, Dinarvand N, Sabaghan M, Azadbakht O, Ataee S, Kharazinejad E, et al. (2024). Diabetes and ovarian cancer: Risk factors, molecular mechanisms and impact on prognosis. Endocrine; 83(1):1-9.
30) Yadav J, Chauhan P, Rawat RK, Pathak SK, Srivastava S. (2024). Syzygium aromaticum-mediated green synthesis of iron oxide nanoparticles for efficient heavy metal removal from aqueous solutions. Journal of the Indian Chemical Society; 101(8):101201.
31) Chaudhary P, Goel B, Ghosh AK. (2012). Antidiabetic activity of Adina cordifolia (Roxb) leaves in alloxan induced diabetic rats. Asian Pacific Journal of Tropical Biomedicine; 2(3):S1630-S2.
32 Durvas Seshian B, Pandian BR, Durai U. (2020). Adina Cordifolia as a corrosion inhibitor–a green approach against mild steel corrosion in 0.5 M sulphuric acid medium. Pigment & Resin Technology; 49(1):63-70.
33) Iqbal PF, Bhat AR, Azam A. (2009). Antiamoebic coumarins from the root bark of Adina cordifolia and their new thiosemicarbazone derivatives. European journal of medicinal chemistry; 44(5):2252-9.
34) IMT G. (2022). Review on pharmacological and phytochemical spectrum of “Traditional medicinal plant Adina Cordifolia” family-Rubiaceae. IJASRD; 7:216.
35) Negi S, Negi A, Mishra MK. Pharmacological and Phytochemical

Vol. 20 (Supplementry Issue 1A), March 2026, ISSN 0973-8916 (Print)., 2230-7303 (Online)
10.5530/ctbp.2026.1s.5

Spectrum of Traditional Medicinal Plant Adina Cordifolia Family-Rubiaceae: A REVIEW.
36) Jayakodi S, Shanmugam R, Almutairi BO, Almutairi MH, Mahboob S, Kavipriya M, et al. (2022). zadirachta indica-wrapped copper oxide nanoparticles as a novel functional material in cardiomyocyte cells: An ecotoxicity assessment on the embryonic development of Danio rerio. Environmental Research; 212:113153.
37 Kouhbanani MAJ, Beheshtkhoo N, Taghizadeh S, Amani AM, Alimardani V. (2019). One-step green synthesis and characterization of iron oxide nanoparticles using aqueous leaf extract of Teucrium polium and their catalytic application in dye degradation. Advances in Natural Sciences: Nanoscience and Nanotechnology; 10(1):015007.
38) Fritsch E, Balan E, Petit S, Juillot F. (2021). Structural, textural, and chemical controls on the OH stretching vibrations in serpentine-group minerals. European Journal of Mineralogy; 33(4):447-62.
39) Menazea A, Ibrahium HA, Awwad NS, (2022). Moustapha ME, Farea M, Bajaber MA. Facile synthesis and high-performance dielectric properties of polyethylene oxide-chitosan-iron oxide nano-composite for electrical applications. Journal of Materials Research and Technology; 18:2273-81.
40) Tahir M, Fakhar-e-Alam M, Atif M, Mustafa G, Ali Z. (2023). Investigation of optical, electrical and magnetic properties of hematite α-Fe2O3 nanoparticles via sol-gel and co-precipitation method. Journal of King Saud University-Science; 35(5):102695.
41) Kamal A, Saba M, Farooq M. (2023). Biocompatible formulations based on mycosynthesized iron oxide nanoparticles: Fabrication, characterization, and biological investigation. Journal of Basic Microbiology; 63(2):156-67.
42 Ebrahimpour S, Esmaeili A, Beheshti S. (2018). Effect of quercetin-conjugated superparamagnetic iron oxide nanoparticles on diabetes-induced learning and memory impairment in rats. International journal of nanomedicine. :6311-24.
43) Shabbir MA, Naveed M, Rehman SU, Ain Nu, Aziz T, Alharbi M, et al. (2023). Synthesis of iron oxide nanoparticles from Madhuca indica plant extract and assessment of their cytotoxic, antioxidant, anti-inflammatory, and anti-diabetic properties via different nanoinformatics approaches. ACS omega; 8(37):33358-66.
44) Daniel AI, Umar MB, Tijani OJ, Muhammad R. (2022). Antidiabetic potentials of green-synthesized alpha iron oxide nanoparticles using stem extract of Securidaca longipedunculata. International Nano Letters; 12(3):281-93.
45 Li H, Su X. (2025). Green formulation of iron nanoparticles by Panicum repens extract for the treatment of gestational diabetes and hepatotoxicity by following the biochemical and stereological parameters. Journal of Science: Advanced Materials and Devices. :100903.
46) Shanmugam R, Munusamy T, Rajaselin A, Govindharaj S. (2024). Exploring the in vitro antidiabetic potential of metal oxide nanoparticles synthesized using lemongrass and mint formulation. Cureus; 16(2).
47) Vignesh Kumar G, Shanmugam R, Deenadayalan P, Manigandan P. (2024). Anticariogenic, Antidiabetic, and Toxicology Evaluation of the Ethanolic Extract of Croton bonplandianum: An In Vitro Study. .
48) Vallinayaki K, Shanmugam R. (2024). Evaluation of antidiabetic activity and cytotoxic effect of strontium nanoparticles synthesized using Mimosa pudica. Journal of Pharmacy and Bioallied Sciences; 16(Suppl 2):S1340-S4.